nature climate change

LETTERS

PUBLISHED ONLINE: 2 MARCH 2015 | DOI: 10.1038/NCLIMATE2550

Optimal stomatal behaviour around the world

Yan-Shih Lin *et al.*†

Stomatal conductance (g_s) is a key land-surface attribute as it links transpiration, the dominant component of global land evapotranspiration, and photosynthesis, the driving force of the global carbon cycle. Despite the pivotal role of g_s in predictions of global water and carbon cycle changes, a global-scale database and an associated globally applicable model of g_s that allow predictions of stomatal behaviour are lacking. Here, we present a database of globally distributed g_s obtained in the field for a wide range of plant functional types (PFTs) and biomes. We find that stomatal behaviour differs among PFTs according to their marginal carbon cost of water use, as predicted by the theory underpinning the optimal stomatal model[1] and the leaf and wood economics spectrum[2,3]. We also demonstrate a global relationship with climate. These findings provide a robust theoretical framework for understanding and predicting the behaviour of g_s across biomes and across PFTs that can be applied to regional, continental and global-scale modelling of ecosystem productivity, energy balance and ecohydrological processes in a future changing climate.

Earth system models (ESMs), which integrate biogeochemical and biogeophysical land-surface processes with physical climate models, have been widely used to demonstrate the importance of land-surface processes in determining climate and to highlight the large uncertainties in quantifying land-surface processes[4–6]. Within the biogeophysical components of land-surface processes, g_s plays a pivotal role because it is a key feedback route for carbon and water exchange between the atmosphere and terrestrial vegetation. Stomata are small pores on leaves whose aperture is actively regulated by plants in response to multiple abiotic and biotic factors, and their conductance is a major determinant of global land evapotranspiration and global water and carbon cycles. Therefore, our ability to model the global carbon and water cycles under a future changing climate depends on our ability to predict g_s globally[7]. Many ESMs at present use an empirical stomatal model to predict g_s and, in the absence of information, assume identical parameter values for all non-water-stressed C_3 and C_4 vegetation. For example, the LPJ model[4] assumes a constant ratio of intercellular to ambient CO_2 concentration (C_i:C_a) of 0.8 for all C_3 vegetation and 0.4 for all C_4 vegetation. The CABLE model[8] uses the empirical stomatal model of Leuning[9] with two sets of parameter values, one for all C_3 vegetation and one for all C_4 vegetation. The CLM 4.0 model[10] uses the empirical stomatal model of Ball *et al.*[11] with three sets of parameter values, one for C_4, one for needle-leaf trees, and a third for all other C_3 vegetation. Although there have been previous synthesis studies on plant stomatal conductance and related traits[3,7,12,13], we lack a global-scale database and an associated globally applicable model of g_s that allows predictions of stomatal behaviour among PFTs and across climatic gradients.

For this study, we compiled a unique global database of field measurements of g_s and photosynthesis suitable for estimating model parameters. We employed a model of optimal stomatal conductance[14] to develop hypotheses for how stomatal behaviour should vary with environmental factors and with plant traits associated with hydraulic function. The optimization premise

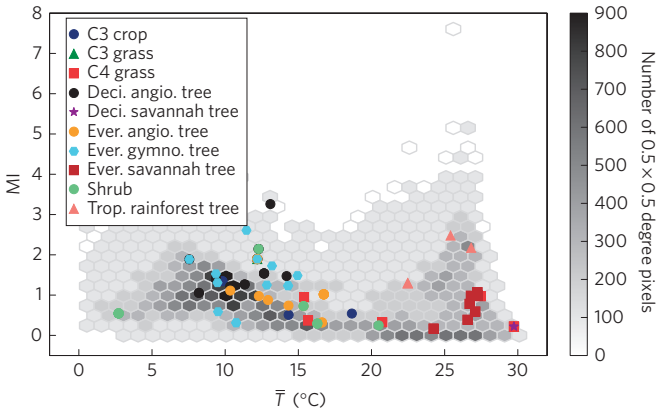

Figure 1 | Climatic space covered by the Stomatal Behaviour Synthesis Database, shown as mean temperature during the period with daily mean temperatures above 0 °C and moisture index. Coloured circles represent climatic space for the database, with different colours indicating different plant functional types. Grey hexagons represent global climatic space for which vegetation is present. The global climatic space data were binned by every 1 °C for temperatures above 0 °C ($\bar{T}$) and every 0.25 for the moisture index (MI). The grey scale bar indicates the number of 0.5 × 0.5 degree pixels for a given binned $\bar{T}$ and MI combination.

underlying this model[1] is that stomata are regulated so as to maximize photosynthesis minus the carbon cost of transpiration, $A-\lambda E$, where λ (mol CO_2 mol^{-1} H_2O) is the carbon cost per unit water used by the plant. Intuitively, λ represents the plant's exchange rate between carbon uptake and water use: a high value of λ indicates that transpiration is costly in carbon terms, meaning that the plant is likely to be conservative in its use of water. From this premise, the model predicts that g_s should be related to photosynthesis, vapour pressure deficit and atmospheric CO_2 concentration, with a single slope parameter, g_1, that is inversely proportional to $\sqrt{\lambda}$ (refs 1,14,15). The slope parameter g_1 is readily estimated from experimental data (Methods) and can be used as an index of λ, where small values of g_1 indicate a high λ. The model also predicts that, under constant environmental conditions, g_1 should be inversely related to plant water-use efficiency[14].

We hypothesized that variation in λ, and therefore in g_1, values among climate zones and PFTs can be predicted from plant carbon–water relations. Specifically, we hypothesized that:

(1) g_1 values among PFTs should vary according to the cost of stemwood construction per unit water transport, such that C_3 herbaceous species should have the largest g_1 (that is, be least water-use efficient), followed by angiosperm trees and gymnosperm trees. We predicted that angiosperm trees would have larger g_1 than gymnosperms due to their higher sapwood permeability, which yields a lower carbon cost of construction per unit water transported. Herbaceous C_4 species form a special case. Due to the different shape of the photosynthesis—g_s response in C_4 plants, the optimal stomatal theory predicts that, for the same λ value, g_1 should

† A full list of authors and affiliations appears at the end of the paper.

be approximately one-fifth of what it would be for C_3 species (see Supplementary Note). We therefore predicted that C_4 plants would have the lowest g_1 and be the most water-use efficient PFT.

(2) For trees, λ should increase with wood density, due to the higher cost of wood construction[16] per unit water transported. Therefore, within both angiosperms and gymnosperms, species with larger wood densities should lead to higher carbon cost per unit water transport (smaller values of g_1).

(3) Low soil water availability should increase λ, so plants adapted to dry environments should have larger λ and lower g_1.

(4) g_1 values should increase with growth temperature for two reasons. First, in the derivation of the optimal stomatal model[14], g_1 is approximately proportional to Γ^* (the CO_2 compensation point in absence of photorespiration). As Γ^* is exponentially dependent on temperature[17], g_1 should increase with temperature. Second, the viscosity of water decreases with increasing temperature, making it less costly to transport water, leading to an increased g_1 (ref. 15).

To test these hypotheses, we collated a globally distributed database of g_s and photosynthesis, including 56 field studies covering a wide range of biomes from Arctic tundra, boreal and temperate forest to tropical rainforest (Supplementary Table 2). We estimated the model coefficient, g_1, from observations of leaf-level gas exchange (g_s and rates of net photosynthesis, see Methods) and environmental drivers (vapour pressure deficit and ambient CO_2 concentration). Next, we correlated estimates of g_1 with two climatic variables: $\bar{T}$, which is the mean temperature over the period when daily mean temperatures are above 0 °C, and a moisture index (MI), which is calculated as the ratio of mean annual precipitation to the equilibrium evapotranspiration. Both $\bar{T}$ and MI were derived from observed long-term meteorological data as proxies of the temperature and water availability that are relevant to plant physiological functions for each site[18]. Our database included a range of $\bar{T}$ from 2.7 to 29.7 °C and a range of MI from 0.17 to 3.26, representing the majority of the climatic space for vegetation-covered land surfaces (Fig. 1). We then tested how g_1 varies with MI and $\bar{T}$ across PFTs and biomes.

Table 1 | Analysis of variance table for g_1 as a function of MI and $\bar{T}$.

	Model				
Variables	**no. d.f.**	**den d.f.**	***F*-value**	***p*-value**	**Marginal R^2**
Intercept	1	97	76.97	<0.001	0.35
MI	1	97	13.38	0.004	Conditional R^2
$\bar{T}$	1	97	7.18	0.009	0.89
MI × $\bar{T}$	1	97	2.61	0.110	

no. d.f.: degrees of freedom in the numerator; den d.f.: degrees of freedom in the denominator.

We found a clear pattern of g_1 variation among different PFTs, with evergreen savannah trees (all angiosperms) having the largest g_1, followed by C_3 crops and grasses, angiosperm trees (other than evergreen savannah trees), gymnosperm trees, and C_4 grasses (Supplementary Table 3 and Fig. 2). For angiosperm trees, g_1 was negatively correlated with wood density, although we did not find a correlation for gymnosperm species (Fig. 3). Across the entire

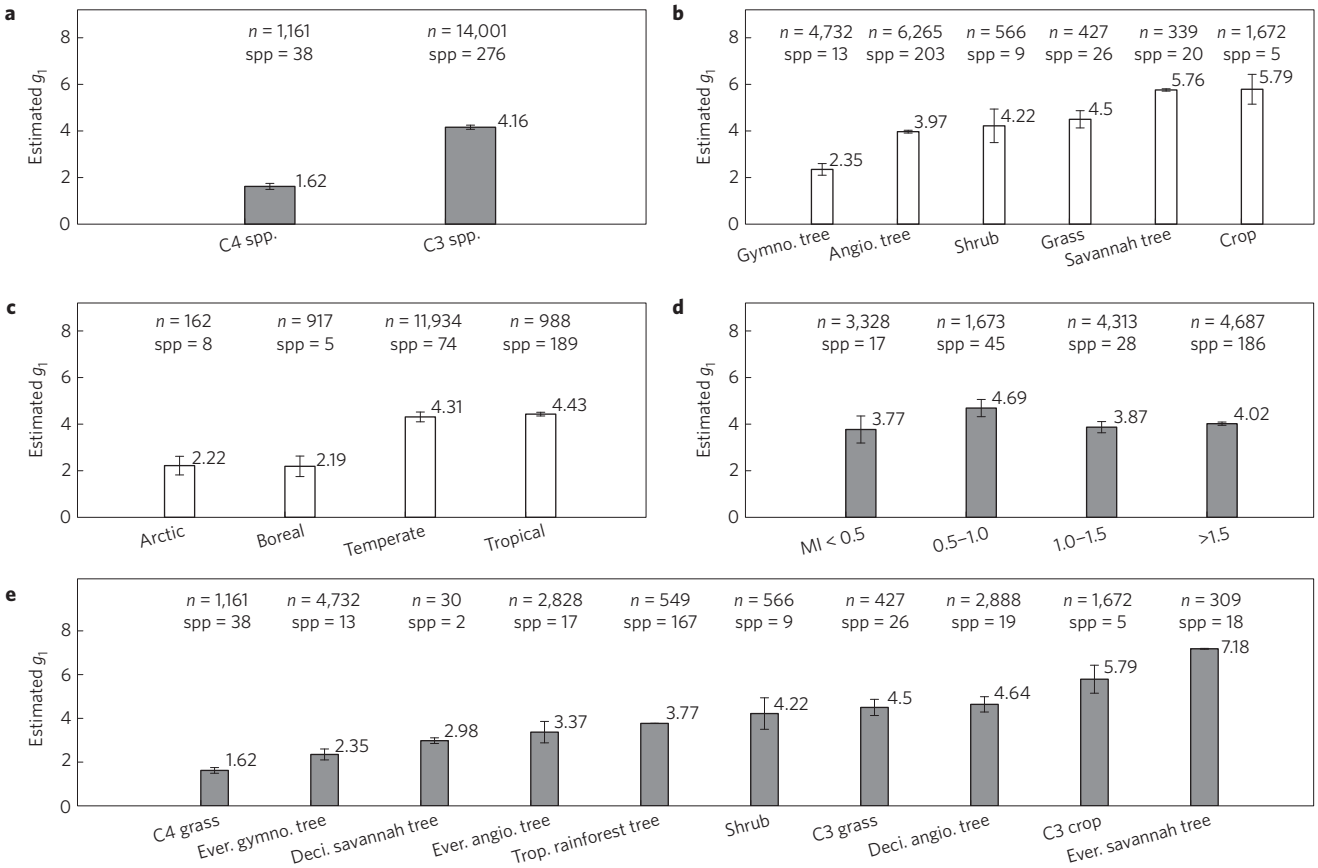

Figure 2 | Mean g_1 values for plant functional types defined by different classification schemes. Each bar represents the mean values ± 1SE of g_1 from the stomatal model fitted using a nonlinear mixed-effects model assuming species as a random effect. The sample sizes (n) are the number of measurements. In the case of diurnal measurements, measurements might be done on the same leaf but under different environmental conditions. Species number (spp) indicates the number of the species in each group. Panels **b**–**d** include C_3 species data only.

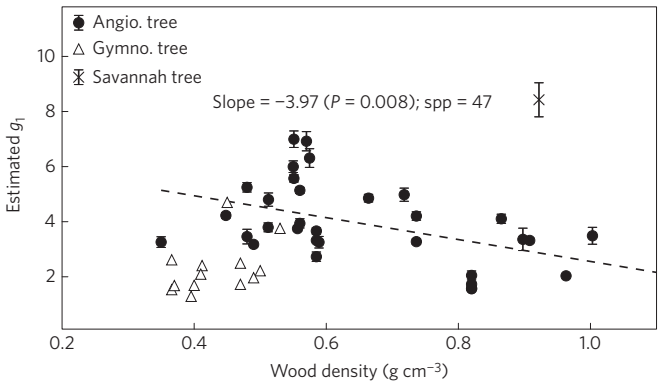

Figure 3 | Relationship between g_1 and wood density for angiosperm and gymnosperm trees. Savannah tree species (all of which were angiosperms) are indicated separately. Each data point represents mean ± 1SE of g_1 for an individual species fitted with a nonlinear regression model. A linear regression line was fitted only for angiosperm trees due to the lack of a significant linear relationship for gymnosperm trees. The fitted linear regression relationship between g_1 and wood density for angiosperm trees is: $g_1 = -3.97*\mathrm{WD} + 6.53$ ($P = 0.0008$, $R^2 = 0.21$). Wood density data were obtained from Global Wood Density Database[2,29] and are available for 47 species in the Stomatal Behaviour Synthesis Database. The wood density database is a collection of published data based on actual measurements.

data set, g_1 significantly increased with $\bar{T}$ and MI. When evaluated as a bivariate relationship, we observed that there was a weak interactive effect of temperature and moisture availability on g_1 (Table 1; $p = 0.11$): in wet environments, g_1 was largest at sites with high $\bar{T}$, but it varied with $\bar{T}$ to a smaller degree across dry environments (Table 1 and Fig. 4).

Our results supported most of our hypotheses for how g_1 should vary among PFTs (hypothesis 1). We predicted that variation in g_1 among PFTs would reflect differences in the carbon cost of water use for different PFTs, which in turn is a general result of different strategies for resource allocation[3,15]. Long-lifespan PFTs, such as gymnosperm trees, must invest more in building support and defence structures relative to short-lifespan PFTs, such as grasses, so that they can survive many years of biotic and abiotic stress. On the basis of this higher construction cost, we predicted a more conservative water-use strategy in trees (lower g_1) than in C_3 grasses (higher g_1), and this was observed in the database. However, evergreen savannah trees formed an exception, with a surprisingly large g_1 relative to expectations based on wood density and biome MI. The large g_1 in the evergreen savannah trees may be related to the fact that these species have several hydraulic functional traits that allow them to have a less conservative water-use strategy. These hydraulic functional traits include: deep roots to access groundwater, large sapwood area to leaf area ratios[19], and dry-season declines in total leaf area to balance increased atmospheric aridity[20]. In addition, there may be seasonal shifts in λ from wet to dry season, reflecting changes in the relative availability of water. Seasonal measurements suggest dry-season g_1 is lower than wet-season g_1 (Supplementary Fig. 3). This special case of evergreen savannah trees is worthy of further investigation.

We found a significant negative relationship between g_1 and wood density among angiosperm trees (Fig. 3; excluding savannah angiosperm trees) which supported hypothesis 2. A larger wood

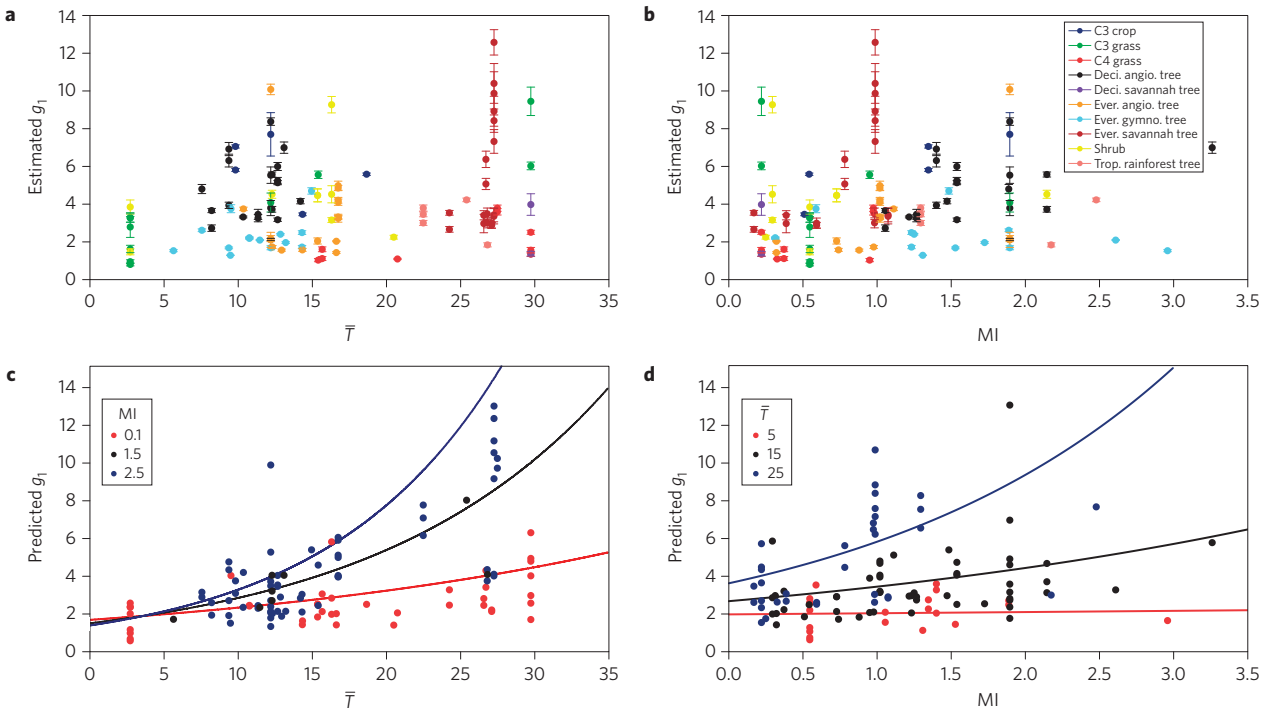

Figure 4 | Estimated and predicted g_1 as a function of $\bar{T}$ and MI. a,**b**, Relationship between estimated g_1 and mean temperature during the period with daily mean temperatures above 0 °C ($\bar{T}$; °C) (**a**) and moisture index (MI) (**b**) at experimental sites among species across different plant functional types (PFTs). Each data point represents the mean ± 1SE of g_1 for individual species fitted with a nonlinear regression model. Classification of plant functional types are shown in Fig. 2e. **c**,**d**, Predicted g_1 under different ranges of MI (**c**) and $\bar{T}$ (**d**) presented as a partial regression plot. Predictions in **c** and **d** are from a weighted linear mixed-effects model for $\log(g_1)$ using the inverse of the SE of g_1 as weights to account for the uncertainty of g_1 fitting and assuming PFTs as a random effect to account for the differences in intercept among PFTs. Coloured lines represent the predicted g_1 based on fitted model coefficients (Supplementary Table 5). Coloured dots represent the partial regression predictions at a given fixed MI or $\bar{T}$ level.

density is highly correlated with other hydraulic traits that are advantageous for plants to avoid hydraulic failure and to sustain more negative sapwood water pressures during periods of soil water deficit[21]. Such an investment in wood density comes at the expense of a reduced capacity for stem water storage, reduced sapwood conductivity and an increased carbon cost of construction per unit volume[22–24], and thus was expected to lead to a more conservative water-use strategy, as we found for angiosperms. However, we did not find such a relationship among gymnosperm trees. This lack of correlation may be due to the limited variability in wood density in gymnosperms. There are significant differences in the anatomical structure of sapwood water transport between angiosperms and gymnosperms. The majority of angiosperm trees have evolved to separate the water transport structure (that is, vessels) from the mechanical support structure, while gymnosperm trees do not have such a functional differentiation, as tracheids are used for both water transport and mechanical support[2,21]. Therefore, wood density is a good proxy for quantifying the trade-offs between transport and support investments for angiosperm trees, but not for gymnosperm trees[2]. The distinct differences in water-use strategy between angiosperm trees and gymnosperm trees (Fig. 2) is consistent with a recent observation that angiosperms maintain a much smaller hydraulic safety margin than gymnosperms[25]; consequently, angiosperms allow some loss of hydraulic conductivity—a risk-tolerant strategy—while gymnosperms minimize this loss. This evolutionary development confers an advantage to angiosperm trees by allowing them to use water in a less conservative way, thereby increasing their carbon gain relative to gymnosperm trees.

Our results supported our hypotheses regarding g_1 variation with soil moisture stress and temperature (hypotheses 3 and 4) and demonstrated different degrees of responses in g_1 between MI and $\bar{T}$. These differing responses demonstrate plant coordination of resource allocation strategies along two climatic gradients, a relationship that has been mostly ignored in many ESMs at present (Fig. 4). Such relationships are not surprising as the two climatic factors affect λ and Γ^* in different directions between warm/dry and warm/wet environments: in a warm/wet environment, Γ^* increases because of higher temperature and λ decreases because of lower moisture stress, leading to higher g_1. However, in a warm/dry environment, higher temperature still promotes the increase of Γ^*, but moisture stress also increases λ, which means g_1 would increase to a smaller degree than in a warm/wet environment. A further explanation is that plants growing in dry environments are likely to be more hydraulically constrained by the need to avoid xylem embolism than those growing in wet environments, and thus there should be less variation in g_1 with other factors.

Our study demonstrates a robust, process-based framework that can be applied at different spatial scales for understanding and predicting the behaviour of stomatal conductance across biomes and across PFTs. We analysed a global stomatal behaviour data set along two major climatic axes, providing a step forward in our understanding of stomatal behaviour in different environments. Our findings will allow the ESM community to move on from using empirical stomatal models with tuned parameters[4,8,10] to using a more robust, theory-derived optimal stomatal model with meaningful parameters. In addition, we provide a valuable stomatal behaviour database that can be used to parameterize g_s among PFTs and can be applied directly within ESMs to simulate ecosystem productivity and ecohydrological responses to future climate scenarios across regional, continental and global scales.

Methods

Source of data. We synthesized published and unpublished leaf-level gas exchange data for a wide range of PFTs and biomes (Supplementary Table 2). In all cases, measurements were made using leaf cuvette chambers that measure water vapour and CO_2 fluxes from leaves. We used only data sets including instantaneous measurements under ambient field conditions. We did not include any data sets from standard response curve measurements, such as CO_2 response curves or light response curves. Our database covers 314 species from 56 experimental sites around the world, with 17 sites from Australasia, 15 sites from Europe, 14 sites from North America, six sites from Asia, three sites from South America and one site from Africa. Site latitudes range from 42.9° S to 72.3° N, although the majority of the sites are within the temperate zone ($n=35$; latitude range between 23.5° and 55° and between −23.5° and −55°), followed by tropical zone ($n=14$; latitude range between −23.5° and 23.5°), boreal zone ($n=6$; latitude range between 55° and 66.5°) and Arctic zone ($n=1$; latitude range above 66.5°). The whole database is publicly available and can be downloaded from the data repository (http://figshare.com/articles/Optimal_stomatal_behaviour_around_the_world/1304289).

We derived MI and $\bar{T}$ from Climate Research Unit climatology data (CRU CL1.0; ref. 26) from 1960 to 1990 with a modified version of the STASH model[27] at a grid resolution of 0.5°. In this derivation, $\bar{T}$ was calculated as the ratio of the annual sum of linear interpolated daily temperatures above 0 °C (growing degree days) to the length of this period; MI was calculated as the ratio of mean annual precipitation to the equilibrium evapotranspiration (E_{eq}). We estimated E_{eq} from monthly mean temperature and net radiation (calculated from monthly mean percentage of cloud cover)[27]. The Sea-WiFS fAPAR (fraction absorbed photosynthetically active radiation) product[28] was used to determine areas with green vegetation cover at a grid resolution of 0.5°, as shown in Fig. 1. The wood density data were obtained from the Global Wood Density Database[2,29].

Data analysis. We used leaf-level gas exchange data sets which were collected with standard portable gas exchange instruments. We used data measured at a photosynthetic photon flux density (PPFD) $>0\,\mu mol\,m^{-2}\,s^{-1}$, and only data collected from the top third of the canopy. In all cases, species were grown under ambient environmental conditions and were not subjected to any treatments, such as elevated CO_2, temperature, or drought treatments. We employed the optimal stomatal model[14]:

$$g_s = 1.6\left(1+\frac{g_1}{\sqrt{D}}\right)\frac{A}{C_a} \quad (1)$$

where D is vapour pressure deficit (kPa), A is net photosynthesis rate ($\mu mol\,m^{-2}\,s^{-1}$), C_a is CO_2 concentration at the leaf surface (ppm), and g_1 is the model coefficient. We used a nonlinear mixed-effect model to estimate the model slope coefficient, g_1, for each group separately for various classification schemes, as shown in Fig. 2. In this model, individual species were assumed to be the random effect to account for the differences in the g_1 slope among species within the same group.

In the original derivation of the optimal stomatal model[14], an intercept term g_0 was added to equation (1) to ensure correct behaviour of C_i as A approaches zero, following Leuning[9]. This term is often thought of as representing the minimum, or cuticular stomatal conductance. Here, we did not fit this term for several reasons. First, fitted values of g_0 and g_1 tend to be correlated, meaning that it is not possible to compare values of g_1 across data sets when g_0 has also been fitted. Second, it is not clear that adding an intercept to equation (1) is the correct way to handle a minimum stomatal conductance, because this affects all predictions of g_s, not just those where A is close to zero. It may be more appropriate to include the g_0 term as a minimum bound to equation (1).

To test how g_1 varies with climatic variables (that is, MI and $\bar{T}$), we first estimated g_1 for each species using a nonlinear regression model (Supplementary Table 4). We then used a weighted linear mixed-effect model to test the relationship between g_1, MI and $\bar{T}$. We fitted the model as:

$$\log(g_1) \sim \mathrm{MI} + \bar{T} + \mathrm{MI}\times\bar{T}$$

using the inverse of the standard error (SE) of g_1 as the weighting scale to account for the uncertainty of g_1 fitting and assuming PFTs as the random effect to account for the differences in intercept among PFTs. To evaluate the goodness of fit of the linear mixed-effect models, we calculated both the marginal R^2 to quantify the proportion of variance explained by the fixed factors alone and the conditional R^2 to quantify the proportion of variance explained by both the fixed and random factors[26]. The relationship between g_1 and wood density was tested with a simple linear regression model. All model estimations and statistical analyses were performed with R 3.1.0 (refs 30–32).

Received 16 August 2014; accepted 16 January 2015; published online 2 March 2015

References

1. Cowan, I. R. & Farquhar, G. D. Stomatal function in relation to leaf metabolism and environment. *Symp. Soc. Exp. Biol.* **31,** 471–505 (1977).

2. Chave, J. *et al.* Towards a worldwide wood economics spectrum. *Ecol. Lett.* **12,** 351–366 (2009).
3. Wright, I. J., Falster, D. S., Pickup, M. & Westoby, M. Cross-species patterns in the coordination between leaf and stem traits, and their implications for plant hydraulics. *Physiol. Plant.* **127,** 445–456 (2006).
4. Sitch, S. *et al.* Evaluation of ecosystem dynamics, plant geography and terrestrial carbon cycling in the LPJ dynamic global vegetation model. *Glob. Change Biol.* **9,** 161–185 (2003).
5. Cao, M. & Woodward, F. I. Dynamic responses of terrestrial ecosystem carbon cycling to global climate change. *Nature* **393,** 249–252 (1998).
6. Friedlingstein, P. *et al.* Climate–carbon cycle feedback analysis: Results from the C4MIP model intercomparison. *J. Clim.* **19,** 3337–3353 (2006).
7. Schulze, E-D., Kelliher, F. M., Korner, C., Lloyd, J. & Leuning, R. Relationships among maximum stomatal conductance, ecosystem surface conductance, carbon assimilation rate, and plant nitrogen nutrition: A global ecology scaling exercise. *Annu. Rev. Ecol. Syst.* **25,** 629–660 (1994).
8. Kowalczyk, E. A. *et al. The CSIRO Atmosphere Biosphere Land Exchange (CABLE) Model for Use in Climate Models and as an Offline Model* (CSIRO Marine and Atmospheric Research, 2006).
9. Leuning, R. A critical appraisal of a combined stomatal-photosynthesis model for C3 plants. *Plant Cell Environ.* **18,** 339–355 (1995).
10. Oleson, K. W. *et al. Technical Description of Version 4.0 of the Community Land Model (CLM)* (NCAR, 2010).
11. Ball, J. T., Woodrow, I. E. & Berry, J. A. *Progress in Photosynthesis Research* (Martinus Nijhoff Publishers, 1987).
12. Kattge, J. *et al.* TRY—a global database of plant traits. *Glob. Change Biol.* **17,** 2905–2935 (2011).
13. Lloyd, J. & Farquhar, G. 13C discrimination during CO_2 assimilation by the terrestrial biosphere. *Oecologia* **99,** 201–215 (1994).
14. Medlyn, B. E. *et al.* Reconciling the optimal and empirical approaches to modelling stomatal conductance. *Glob. Change Biol.* **17,** 2134–2144 (2011).
15. Prentice, I. C., Dong, N., Gleason, S. M., Maire, V. & Wright, I. J. Balancing the costs of carbon gain and water transport: Testing a new theoretical framework for plant functional ecology. *Ecol. Lett.* **17,** 82–91 (2014).
16. Héroult, A., Lin, Y-S., Bourne, A., Medlyn, B. E. & Ellsworth, D. S. Optimal stomatal conductance in relation to photosynthesis in climatically contrasting Eucalyptus species under drought. *Plant Cell Environ.* **36,** 262–274 (2013).
17. Bernacchi, C. J., Singsaas, E. L., Pimentel, C., Portis, A. R. Jr & Long, S. P. Improved temperature response functions for models of Rubisco-limited photosynthesis. *Plant Cell Environ.* **24,** 253–259 (2001).
18. Harrison, S. P. *et al.* Ecophysiological and bioclimatic foundations for a global plant functional classification. *J. Veg. Sci.* **21,** 300–317 (2010).
19. Gotsch, S. *et al.* Allocation to leaf area and sapwood area affects water relations of co-occurring savanna and forest trees. *Oecologia* **163,** 291–301 (2010).
20. Eamus, D., O'Grady, A. P. & Hutley, L. Dry season conditions determine wet season water use in the wet—tropical savannas of northern Australia. *Tree Physiol.* **20,** 1219–1226 (2000).
21. Hacke, U. G., Sperry, J. S., Pockman, W. T., Davis, S. D. & McCulloh, K. A. Trends in wood density and structure are linked to prevention of xylem implosion by negative pressure. *Oecologia* **126,** 457–461 (2001).
22. Meinzer, F. C., James, S. A., Goldstein, G. & Woodruff, D. Whole-tree water transport scales with sapwood capacitance in tropical forest canopy trees. *Plant Cell Environ.* **26,** 1147–1155 (2003).
23. Bucci, S. J. *et al.* Functional convergence in hydraulic architecture and water relations of tropical savanna trees: From leaf to whole plant. *Tree Physiol.* **24,** 891–899 (2004).
24. Sperry, J. S., Meinzer, F. C. & McCulloh, K. A. Safety and efficiency conflicts in hydraulic architecture: Scaling from tissues to trees. *Plant Cell Environ.* **31,** 632–645 (2008).
25. Choat, B. *et al.* Global convergence in the vulnerability of forests to drought. *Nature* **491,** 752–755 (2012).
26. New, M., Hulme, M. & Jones, P. Representing twentieth-century space–time climate variability. Part I: Development of a 1961–90 mean monthly terrestrial climatology. *J. Clim.* **12,** 829–856 (1999).
27. Gallego-Sala, A. *et al.* Bioclimatic envelope model of climate change impacts on blanket peatland distribution in Great Britain. *Clim. Res.* **45,** 151–162 (2010).
28. Gobron, N. *et al.* Evaluation of fraction of absorbed photosynthetically active radiation products for different canopy radiation transfer regimes: Methodology and results using Joint Research Center products derived from SeaWiFS against ground-based estimations. *J. Geophys. Res.* **111,** D13110 (2006).
29. Zanne, A. E. *et al. Data from: Towards a Worldwide Wood Economics Spectrum* (Dryad Data Repository, 2009).
30. R Core Team *R: A language and Environment for Statistical Computing* (R Foundation for Statistical Computing, 2014).
31. Pinheiro, J., Bates, D., DebRoy, S., Sarkar, D. & Team, R. C. *nlme: Linear and Nonlinear Mixed Effects Models R Package Version 3.1-117* (R Foundation for Statistical Computing, 2014).
32. Breheny, P. & Burchett, W. *Visreg: Visualization of Regression Models R Package Version 2.0-5* (R Foundation for Statistical Computing, 2014).

Acknowledgements

This research was supported by the Australian Research Council (ARC MIA Discovery Project 1433500-2012-14). A.R. was financially supported in part by The Next-Generation Ecosystem Experiments (NGEE-Arctic) project, which is supported by the Office of Biological and Environmental Research in the Department of Energy, Office of Science, and through the United States Department of Energy contract No. DE-AC02-98CH10886 to Brookhaven National Laboratory. M.O.d.B. acknowledges that the Brassica data were obtained within a research project financed by the Belgian Science Policy (OFFQ, contract number SD/AF/02) and coordinated by K. Vandermeiren at the Open-Top Chamber research facilities of CODA-CERVA (Tervuren, Belgium).

Author contributions

Y-S.L., B.E.M. and R.A.D. conceived, designed and analysed the data and wrote the manuscript. I.C.P. contributed to study design and comments on the manuscript. R.A.D., B.E.M. and S.B. contributed to the implementation of the optimal stomatal model for C_4 species in the Supplementary Note. H.W. wrote the R script for the implementation of the STASH model and commented on the manuscript. All other authors contributed data and commented on the manuscript.

Additional information

Supplementary information is available in the online version of the paper. Reprints and permissions information is available online at www.nature.com/reprints. Correspondence and requests for materials should be addressed to Y-S.L.

Competing financial interests

The authors declare no competing financial interests.

Yan-Shih Lin[1]*, Belinda E. Medlyn[1], Remko A. Duursma[2], I. Colin Prentice[1,3], Han Wang[1], Sofia Baig[1], Derek Eamus[4], Victor Resco de Dios[5], Patrick Mitchell[6], David S. Ellsworth[2], Maarten Op de Beeck[7], Göran Wallin[8], Johan Uddling[8], Lasse Tarvainen[9], Maj-Lena Linderson[10], Lucas A. Cernusak[11], Jesse B. Nippert[12], Troy W. Ocheltree[13], David T. Tissue[2], Nicolas K. Martin-StPaul[14], Alistair Rogers[15], Jeff M. Warren[16], Paolo De Angelis[17], Kouki Hikosaka[18], Qingmin Han[19], Yusuke Onoda[20], Teresa E. Gimeno[2], Craig V. M. Barton[2], Jonathan Bennie[21], Damien Bonal[22], Alexandre Bosc[23,24], Markus Löw[25], Cate Macinins-Ng[26], Ana Rey[27], Lucy Rowland[28], Samantha A. Setterfield[29], Sabine Tausz-Posch[25], Joana Zaragoza-Castells[28], Mark S. J. Broadmeadow[30], John E. Drake[2], Michael Freeman[31], Oula Ghannoum[2], Lindsay B. Hutley[29], Jeff W. Kelly[1], Kihachiro Kikuzawa[32], Pasi Kolari[33], Kohei Koyama[32,34], Jean-Marc Limousin[35], Patrick Meir[28], Antonio C. Lola da Costa[36], Teis N. Mikkelsen[37], Norma Salinas[38,39], Wei Sun[40] and Lisa Wingate[23]

[1]Department of Biological Sciences, Macquarie University, North Ryde, New South Wales 2109, Australia. [2]Hawkesbury Institute for the Environment, University of Western Sydney, Penrith, New South Wales 2751, Australia. [3]AXA Chair of Biosphere and Climate Impacts, Grand Challenges in Ecosystems and the Environment and Grantham Institute—Climate Change and the Environment, Department of Life Sciences, Imperial College London, Silwood Park Campus, Buckhurst Road, Ascot SL5 7PY, UK. [4]School of the Environment, University of Technology, Sydney, New South Wales 2007, Australia.

[5]Ramón y Cajal Programme, Department of Crop and Forest Sciences-AGROTECNIO Center, Universitat de Lleida, E 25198 Lleida, Spain. [6]CSIRO Ecosystem Sciences, Sandy Bay, Tasmania 7005, Australia. [7]Research Group Plant and Vegetation Ecology, University of Antwerp, Wilrijk 2610, Belgium. [8]Department of Biological and Environmental Sciences, University of Gothenburg, Göteborg 40530, Sweden. [9]Department of Forest Ecology and Management, Swedish University of Agricultural Sciences, Umeå 90183, Sweden. [10]Department of Physical Geography and Ecosystem Science, Lund University, 22362 Lund, Sweden. [11]James Cook University, Cairns, Queensland 4879, Australia. [12]Division of Biology, Kansas State University, Manhattan, Kansas 66505, USA. [13]Department of Forest and Rangeland Stewardship, Colorado State University, Fort Collins, Colorado 80523, USA. [14]Université Paris-Sud, Laboratoire Ecologie, Systématique et Evolution, UMR8079, Orsay F-91405, France. [15]Environmental and Climate Sciences Department, Brookhaven National Laboratory, Upton, New York 11973-5000, USA. [16]Environmental Sciences Division, Oak Ridge National Laboratory, Oak Ridge, Tennessee 37831, USA. [17]Department for Innovation in Biological, Agro-food and Forest systems, University of Tuscia, Via San Camillo de Lellis, Viterbo 01100, Italy. [18]Graduate School of Life Sciences, Tohoku University, Aoba, Sendai 980-8578, Japan. [19]Hokkaido Research Center, Forestry and Forest Products Research Institute (FFPRI), Toyohira, Sapporo, Hokkaido 062-8516, Japan. [20]Division of Environmental Science and Technology, Graduate School of Agriculture, Kyoto University, Oiwake, Kitashirakawa, Kyoto 606-8502, Japan. [21]Environment and Sustainability Institute, University of Exeter, Penryn, TR10 9FE, UK. [22]Institut National de la Recherche Agronomique, Nancy, Champenoux 54280, France. [23]Institut National de la Recherche Agronomique, Villenave d'Ornon F-33140, France. [24]Bordeaux Sciences Agro, UMR 1391 ISPA, Gradignan F-33170, France. [25]Faculty of Veterinary & Agricultural Sciences, University of Melbourne, Creswick, Victoria 3363, Australia. [26]School of Environment, University of Auckland, Auckland 1142, New Zealand. [27]Department of Biogeography and Global Change, MNCN-CSIC, Spanish Scientific Council, Madrid 28006, Spain. [28]School of Geosciences, University of Edinburgh, Edinburgh EH8 9XP, UK. [29]Research Institute for Environment and Livelihoods, Charles Darwin University, Casuarina, Northern Territory 0909, Australia. [30]Climate Change Forest Services, Forestry Commission England, Bristol BD16 1EJ, UK. [31]Department of Ecology, Swedish University of Agricultural Sciences, Uppsala 75007, Sweden. [32]Department of Environmental Science, Faculty of Bioresources and Environmental Sciences, Ishikawa Prefectural University, Ishikawa 921-8836, Japan. [33]Department of Physics, University of Helsinki, Helsinki FI-00014, Finland. [34]Department of Life Science and Agriculture, Obihiro University of Agriculture and Veterinary Medicine, Obihiro, Hokkaido 080-0834, Japan. [35]Department of Biology, University of New Mexico, Albuquerque, New Mexico 87131-0001, USA. [36]Federal University of Para, Belem 66075-110, Brazil. [37]Center for Ecosystems and Environmental Sustainability, Department of Chemical and Biochemical Engineering, Technical University of Denmark, DK-4000 Roskilde, Denmark. [38]Seccion Quimica, PUCP, Lima 15088, Peru. [39]School of Geography, University of Oxford, Oxford OX1 3QY, UK. [40]Institute of Grassland Science, Northeast Normal University, Key Laboratory of Vegetation Ecology, Changchun, Jilin 130024, China. *e-mail: yanshihL@gmail.com